Cross-linking reveals laminin coiled-coil architecture

Gad Armony[a], Etai Jacob[a,b], Toot Moran[a], Yishai Levin[c], Tevie Mehlman[d], Yaakov Levy[a], and Deborah Fass[a,1]

[a]Department of Structural Biology, Weizmann Institute of Science, Rehovot 7610001, Israel; [b]The Mina & Everard Goodman Faculty of Life Sciences, Bar-Ilan University, Ramat-Gan 5290002, Israel; [c]The Nancy and Stephen Grand Israel National Center for Personalized Medicine, Weizmann Institute of Science, Rehovot 7610001, Israel; and [d]Biological Research Support, Weizmann Institute of Science, Rehovot 7610001, Israel

Edited by Peter S. Kim, Stanford University School of Medicine, Stanford, CA, and approved September 28, 2016 (received for review May 25, 2016)

Laminin, an ∼800-kDa heterotrimeric protein, is a major functional component of the extracellular matrix, contributing to tissue development and maintenance. The unique architecture of laminin is not currently amenable to determination at high resolution, as its flexible and narrow segments complicate both crystallization and single-particle reconstruction by electron microscopy. Therefore, we used cross-linking and MS, evaluated using computational methods, to address key questions regarding laminin quaternary structure. This approach was particularly well suited to the ∼750-Å coiled coil that mediates trimer assembly, and our results support revision of the subunit order typically presented in laminin schematics. Furthermore, information on the subunit register in the coiled coil and cross-links to downstream domains provide insights into the self-assembly required for interaction with other extracellular matrix and cell surface proteins.

coiled coil | extracellular matrix | laminin | cross-linking | mass spectrometry

Laminins are network-forming constituents of the extracellular matrix (ECM) (1, 2). They interact with the cell surface and other ECM components to generate a physical and functional framework affecting cell viability, identity, and activity. The laminin family appears to have arisen during the evolution of multicellularity in animals (3), and laminins contribute to a diversity of basement membrane and connective tissue structures in mammals (2). Laminins are studied in the context of development (4), stem cell biology (5), tissue engineering (6), cancer (7), and aging (8). The remarkable structural organization of laminins underlies their important physiological functions.

Laminins are composed of three subunits, α, β, and γ, that assemble into a roughly humanoid form as visualized using rotary shadowing electron microscopy (9). The individual subunits separately form the "head" and two "arms," which are composed of epidermal growth factor (EGF)-like cysteine-rich repeats with globular domains embedded (10) (Fig. 1). Following the head and arms, the three subunits come together to form a long coiled coil, constituting the "body." Additional globular domains unique to the α subunit are the "feet." The laminin head and arms may splay to form a tripod (2), a feature not captured in rotary shadowing images or in diagrams of domain composition. Due to the centrality of laminin in cell–ECM interactions, efforts have been made to analyze the functional regions of the trimer, to determine which α, β, and γ paralogs associate into physiological heterotrimers and to understand how trimers self-assemble into higher-order networks. Laminin fragments have been generated to assess their binding properties (11, 12) and as targets for structure determination by X-ray crystallography (13–20).

Despite this progress, few insights into the overall 3D architecture of laminin have been made in the past few decades, and certain regions of the complex have been neglected as targets of structural techniques. In particular, no structure has been determined for any segment of the laminin coiled coil, which spans more than 750 Å and is the backbone of the laminin quaternary structure. Because the regions of high coiled-coil propensity in α, β, and γ are similar in length, their alignment can be roughly surmised. However, structural deviations in the coiled coil have been suggested to occur (21). More fundamentally, the order of the three subunits has remained ambiguous since evidence for a coiled coil in laminin was presented (22, 23). An analysis based on charged residues in laminin sequences led to the proposal that α, β, and γ are arranged in a clockwise manner when viewed from the carboxyl terminus (24); this order is widely adopted in seminal reviews on laminin structure and function (10, 25, 26). However, other investigators have interpreted biochemical results in the context of a model with the opposite order (27). Clearly, gaps remain in our appreciation of the laminin assembly.

Cross-linking analyzed by MS is a strategy for determining the spatial organization of protein quaternary structures (28, 29). This technique is particularly suitable for elongated protein assemblies such as coiled coils (30), which have high surface-to-volume ratios. The laminin coiled coil is rich in amino acids with cross-linkable functional groups (Fig. 1). Furthermore, coiled coils have well-defined degrees of freedom: oligomeric state, subunit register (i.e., the relative positions of the subunits along the coiled-coil axis), pitch, interface angle, and the order of chains in a hetero-oligomer. Benefiting from the parameterization of coiled-coil geometry, a computational model for laminin subunit association was evaluated under constraints from the cross-linking data. This analysis illuminated previously inaccessible aspects of the laminin quaternary structure. Coupled with information from low resolution electron microscopy and laminin fragment crystallization, a complete picture of the laminin structure is beginning to emerge.

Results

Cross-Linking of the Laminin Heterotrimer. Mouse laminin-111 [laminin isotype (31) containing the α1, β1, and γ1 paralogs, hereafter laminin] was treated with isotopic mixtures, differing by 12.076 Da, of the cross-linkers bis(sulfosuccinimidyl)suberate (BS3) and suberic acid dihydrazide (SDH) to target primary amine and carboxylic acid

Significance

Large, fibrous, and flexible extracellular matrix proteins are integral to development and maintenance of tissues in the body. Laminin is an extracellular matrix component that provides a physical substrate for cell adhesion and induces signaling pathways that maintain cell health and functionality. Despite the physiological importance of laminin, major gaps remain in our understanding of how its three subunits come together to form the characteristic cross-shaped laminin structure. Laminin was treated with chemicals that link amino acids close in space, providing a map of the subunit arrangement and correcting previous suppositions made on the basis of amino acid sequence inspection alone.

Author contributions: G.A., Y. Levy, and D.F. designed research; G.A., E.J., T. Moran, Y. Levin, T. Mehlman, and D.F. performed research; G.A., E.J., Y. Levin, and D.F. analyzed data; and G.A. and D.F. wrote the paper.

The authors declare no conflict of interest.

This article is a PNAS Direct Submission.

Freely available online through the PNAS open access option.

Data deposition: The mass spectrometry proteomics data have been deposited to the ProteomeXchange Consortium via the PRIDE partner repository (dataset identifier PXD004898).

[1]To whom correspondence should be addressed. Email: deborah.fass@weizmann.ac.il.

This article contains supporting information online at www.pnas.org/lookup/suppl/doi:10.1073/pnas.1608424113/-/DCSupplemental.

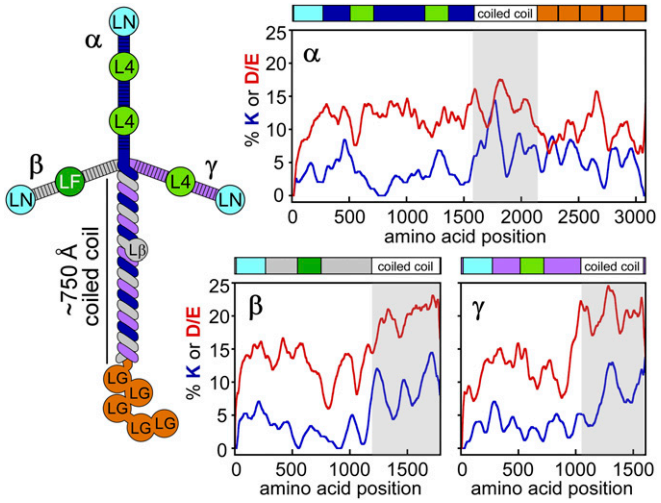

Fig. 1. Laminin domains and cross-linkable side chains. (*Left*) Laminin subunits are labeled α, β, and γ. Domains are labeled according to convention (10). (*Right*) Percentages of primary amine-bearing (K, blue) and carboxylic acid-bearing (D/E, red) side chains were calculated using a sliding window of 40 amino acids, smoothed over 100 amino acids. Coiled-coil regions are shaded.

groups, respectively. Cross-linked laminin was digested proteolytically and subjected to liquid chromatography and tandem MS. Parent ion spectra (MS1) of cross-linked peptides identified from the isotope fingerprint were selected for analysis of fragmentation (MS2) data, which were assigned using xQuest (32). All assigned MS2 spectra were then inspected manually. Criteria for rejecting assignments are given in the *SI Materials and Methods*. During SDH data analysis, we observed direct (zero-length) cross-linking of acidic side chains to lysines as a side effect of the coupling reagent, as reported previously (33). Therefore, we performed a reaction in the absence of SDH to obtain additional zero-length links intentionally. With no isotope coding in this case, all MS1 spectra were searched. In all (Dataset S1), we observed 177 reliable, nonredundant BS3 or SDH links, 134 of which were within the coiled-coil, and 47 of these were intersubunit links. We also observed 92 reliable, nonredundant zero-length links, 77 of which were in the coiled coil, and 22 of these were between subunits.

Cross-Link Validation. Most of the cross-linked peptides were in the coiled coil, but some were within or between globular domains and in the EGF-like repeats. Crystal structures of laminin fragments (14, 15, 17, 18) were used to assess the quality of the cross-linking results (Fig. 2). Cross-links within the β subunit LN domain, the LG4–LG5 domains, and an EGF-like repeat were validated based on Protein Data Bank (PDB) ID codes 4AQS, 2JD4, and 1NPE, respectively. Cross-links within the LG1, LG2, and LG3 domains of the α1 subunit were mapped onto the structure of the mouse α2 paralog (PDB ID code 2WJS), and links within the α1 L4b domain were mapped onto human α2 L4b (PDB ID code 4YEP). Using xWALK (34), the shortest solvent-accessible surface distances (SASDs) between Cβ atoms of linked residues were calculated from the experimentally determined structures listed above. All SASDs for BS3 and SDH links were under 30 Å (average, 17.9 ± 5.0 Å; range, 7.7–29.4 Å), which is less than the maximum of 34 Å for BS3 SASDs in xWALK. Eight SASDs for zero-length cross-links were below 7.3 Å, but three were 14.2, 19.3, and 27.4 Å. Structure inspection indicated that the linked residues are in all cases close in space (<14 Å Euclidean Cβ-Cβ distance) and suggested that minor loop motions or alternate rotamer sampling of intervening residues, expected to occur due to natural protein motions in solution, would permit these direct links to form. The consistency with available crystal structures supports the reliability of the cross-link set.

Assignment of the Subunit Order in the Laminin Coiled Coil. The α, β, and γ subunits can be arranged either clockwise or counter clockwise when viewed down the coiled-coil axis. The order of subunits in the trimer underlies the mechanism of combinatorial assembly of laminin isotypes (35) and therefore is key to understanding the complexity and diversification of the laminin family. We reasoned that the alternative subunit arrangements could be distinguished without knowledge of the register of the three strands. To begin, an ideal trimeric coiled coil was generated using Coiled-Coil Crick Parameterization (36), and the position of each amino acid in the heptad repeat (**a**, **b**, **c**, **d**, **e**, **f**, or **g**) was noted. SASDs with a 34-Å upper limit then were calculated in xWALK for all possible pairs of heptad positions between helices of the model coiled coil (Table S1). In parallel, each laminin coiled-coil residue was assigned its most likely position within a heptad repeat using MARCOIL (37). According to predicted heptad positions, each intersubunit BS3 or SDH cross-link in the coiled coil was given its corresponding SASDs for the clockwise and counter clockwise arrangements (Table S2), and histograms of expected distance were generated for the two competing models (Fig. 3). The cross-linking data overwhelming supported a counter clockwise arrangement of α, β, and γ as viewed from the carboxyl terminus.

Zero-length cross-linking confirmed the subunit order. Many compatible zero-length intersubunit cross-links were observed for a counter clockwise arrangement of α, β, and γ, whereas no compatible links were found for the clockwise arrangement (Table S2). Some cross-links appearing incompatible with either arrangement may involve a rare misassigned cross-link or, more likely, a misassigned heptad position.

Coiled-Coil Register Determination. In addition to the order of subunits around the coiled-coil axis, other fundamental aspects of laminin quaternary structure are the subunit register and the extent of coiled-coil disruptions (21). A primary structural map revealed that most of the intersubunit cross-links are mutually compatible with a continuous coiled coil (Fig. 4). The only major disruption is about 45 residues comprising the Lβ knob (Lβ; Fig. 1), which had to be excised from the alignment to accommodate zero-length cross-links between β and γ on either side of this region (Fig. 4). Two cross-links were observed from Lβ to the α subunit, aligning the knob with the α chain. Another, smaller register shift appears to occur between α1750 and α2007. Specifically, a set of direct cross-links (α1746–β1372, α1746–β1379, and α1750–β1372) is separated from another direct link (α2007–β1659) by 257–261 residues in α and 280–287 residues in β, suggesting a readjustment of two to four heptads in the intervening

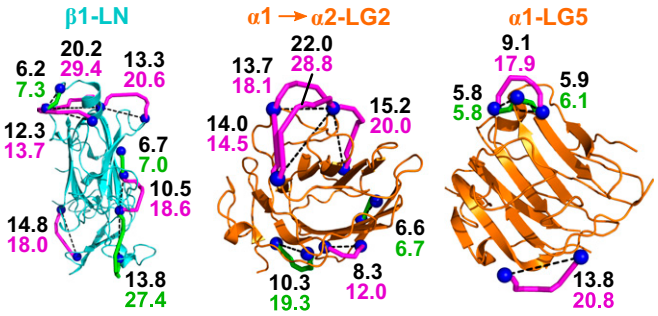

Fig. 2. Validation of laminin cross-linking. Cross-linked positions (Cβ atoms, blue spheres) were mapped onto the structures of the β1 LN and α1 LG5 domains (PDB ID codes 4AQS and 2JD4, respectively) and by homology onto the structure of the α2 LG2 domain (PDB ID code 2WJS). Shortest SASDs are shown as magenta (BS3 and SDH links) or green tubes (zero-length links), and direct Cβ-Cβ distances are shown as black dashed lines. Measures in Ångstrom for the two routes are in the corresponding colors.

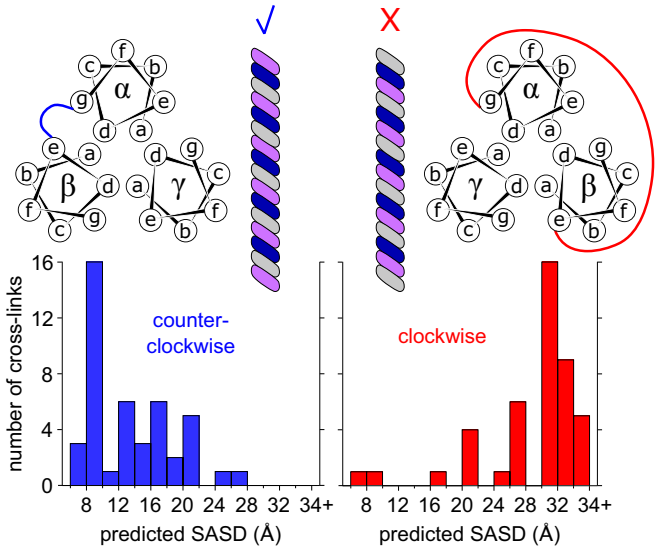

Fig. 3. Cross-linking supports a counterclockwise arrangement of α, β, and γ, viewed from the carboxyl terminus. Schematics of the competing coiled-coil subunit arrangements are shown above. Predicted SASD values based on the likely heptad positions of BS3- and SDH-linked residues are plotted below for each model.

region (Fig. 4). No other gross register shifts appear necessary to account for the data.

Although some heavily cross-linked regions could be directly modeled (Fig. S1 and Table S3), coarse-grained molecular dynamics simulations restrained by the experimental cross-links were used to obtain a global assessment of the subunit register (Fig. 5*A*). The amino acid sequence and MARCOIL heptad position assignments were first threaded onto an ideal trimeric coiled coil. A bead representing each amino acid was placed at the coordinates of its Cα atom in this structure. The resulting model was allowed to relax subject to a force field based on coiled-coil geometry, together with a Lennard–Jones-type potential applied generically between MARCOIL **a** and **d** positions on different chains. This latter feature of the force field accounted for predicted irregularities (e.g., stutters, stammers, and skips) (38) in the heptad repeat by pulling predicted core residues to the core. Following relaxation, the cross-links were applied as bead chains mimicking the dimensions and extensibility of the physical links. Next, multiple simulations were conducted for each of seven different starting alignments differing by four-heptad displacements of individual subunits (for a representative trajectory, see Movie S1). Nearest-neighbor interactions between residues at **a** and **d** positions in each helix pair were extracted from the simulations, yielding the most likely chain register based on the cross-linking data evaluated in the context of the MARCOIL predictions (Fig. 5*B* and Dataset S2). The above procedures were validated using the 120-residue coiled coil of fibrinogen, the current best example of a heterotrimeric coiled coil with known structure (39, 40). Specifically, an artificial set of cross-links compatible with the native fibrinogen structure was able to rectify a register-shifted variant.

During the laminin simulations, the subunit alignment downstream of the Lβ knob, including segments not particularly rich in observed cross-links, converged to a narrow register range. Specifically, 95% of the nearest-neighbor observations fell within a range of two heptads and 80% within one heptad in this region of about 300 amino acids (Fig. 5*C*, Fig. S2, and *SI Materials and Methods*). Another segment of about 100 residues upstream of Lβ also converged with similar precision. The coiled-coil register in the immediate vicinity of Lβ was somewhat more variable in the simulations, tending to absorb the two- to four-heptad register readjustment between the α subunit and the other chains noted above. Variability in the Lβ knob region may reflect real flexibility or may be due to insufficient structural information on the knob itself as input to the simulations. Overall, the simulations are consistent with the manual modeling of specific coiled-coil regions (Fig. S1) and extended the register prediction over most of the laminin coiled coil.

Functional Implications for Laminin Coiled-Coil Register Assignment. The binding site of the heparan sulfate proteoglycan agrin was mapped to residues γ1329 to γ1348 in the laminin coiled coil (11). A coiled-coil framework was necessary for binding activity (11), but further progress in understanding the physical basis for this interaction has been hampered by the unknown register of the three subunits (41). The laminin coiled-coil simulations, restrained by one BS3 and two zero-length links in this region, place the agrin-binding stretch of the γ subunit opposite residues 1863–1880 of the α subunit and 1517–1533 of the β subunit, with a precision of about one heptad. Interestingly, a missing **c** position in the heptad prediction for the α subunit in this region suggests that an irregularity in the coiled coil may contribute to the structural signature recognized by agrin.

Another functionally important region of the laminin coiled coil is its carboxyl terminus, which may guide oligomerization and alignment of the three subunits (42). An accurate register assignment of this region is essential for understanding the physical basis of laminin assembly. We note that the preferred MARCOIL designation for the laminin carboxyl terminus differs by half of a heptad from a previous assignment (27, 42). Approximately 40 amino acids from the carboxyl terminus, we observed zero-length links between β K1746 and both γ E1560 and E1567 (Figs. S1 and S3). To form these links, K1746 would have to be in a **g** position, midway between the two glutamates at **e** positions (Fig. 6). The overall effect is that the β subunit is rotated such that

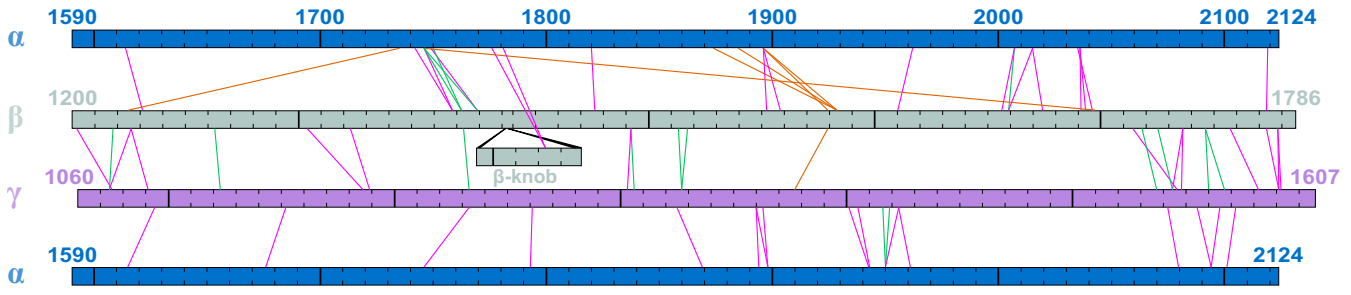

Fig. 4. Map of observed cross-links in the laminin coiled coil. The α subunit is represented twice to show links to both β and γ. BS3/SDH and zero-length cross-links are represented by magenta and green lines, respectively. Orange cross-links appear reliable according to MS data evaluation but are inconsistent with the prevailing register. Figure generated using xiNET (49).

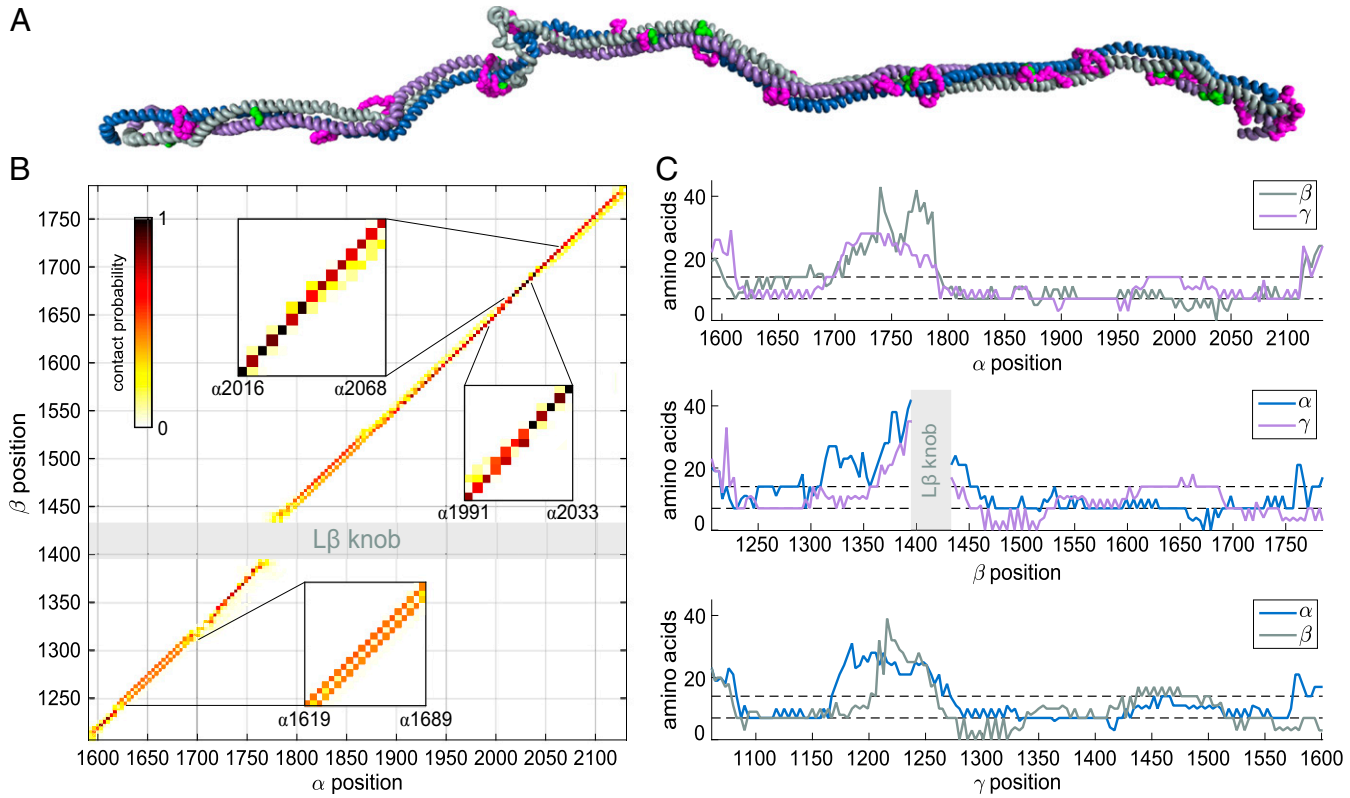

Fig. 5. Laminin coiled-coil register obtained from molecular dynamics simulations subject to cross-linking restraints. (*A*) Snapshot from a simulation (last frame of Movie S1). BS3/SDH and zero-length cross-links are magenta and green, respectively. (*B*) Intersubunit contact map between α and β (α-γ and β-γ maps are in Fig. S2). The map is colored according to the probability for pairs of residues to be found in closest contact from the simulations. Contiguous diagonal contacts indicate a continuous register (e.g., α2016 to α2068). Parallel diagonal sets indicate alternative registers (e.g., α1619 to α1689). A register shift appears as a step between two parallel diagonals (e.g., between α1991 and α2033). (*C*) The uncertainty of the predicted register is estimated for each amino acid residue (*x* axes) by the residue range in another subunit that comprises 95% of observed nearest-neighbor contacts (*y* axes). Dashed lines mark one and two heptads.

what were previously considered **d** and **g** positions (27) become **a** and **d** positions (Fig. 6). The heptad assignment and register fixed by the direct links in turn place a conserved glutamate, β E1748, previously identified as critical for trimer assembly (42), adjacent to a conserved basic residue, α R2092 (Fig. 6 and Fig. S1). In addition, the new heptad assignment places at a **d** position the conserved asparagine β N1750, where it would be adjacent to the highly conserved glutamine γ Q1566, also at a **d** position. It is noteworthy that N1750 is substituted by glycine in laminin β3 chains. It has been observed that β3 forms heterodimeric assembly intermediates with γ2 but not with the γ1 or γ3 paralogs (35). The γ2 subunit differs from γ1 and γ3 at the residue immediately following the conserved Q1566, possessing an arginine instead of a glutamate. Speculatively, this γ2 arginine may compensate for the missing β3 asparagine, a potential factor in formation of β3/γ2 complexes.

Additional Quaternary Structural Insights from Laminin Cross-Links. Many cross-links were observed between β and γ in the carboxyl-terminal region of the coiled coil, but few cross-links were seen coupling α to either β or γ (Fig. 4). Over the last 75 coiled coil residues, the α subunit has fewer cross-linkable residues and is more hydrophobic than the comparable regions of β and γ. The α sequence is also more conserved than the other subunits in non-core positions (Fig. 6). Hydrophobicity and conservation suggest constraints on α chain evolution in addition to maintenance of the coiled coil. Notably, one function of the coiled-coil terminus may be to stabilize the quaternary structural arrangement of the LG domains and support their adhesion functions.

The structures of all five laminin LG domains were previously determined in two sets (14, 15). In the structure of LG1 through LG3, LG1 makes a domain swapping interaction to the LG2–LG3 pair from a different molecule (15), as the tight cloverleaf association of contiguous LG1, LG2, and LG3 domains suggested by electron microscopy (43) was lost. We observed two cross-links between LG1 and LG2–LG3: a zero-length link between LG1 and LG2, and an SDH link between LG1 and the LG2–LG3 junction. By use of these links as restraints, docking with HADDOCK (44) restored the cloverleaf arrangement (Fig. S4). In addition to the cross-links between LG domains, four distinct cross-links tethered the LG domains to the coiled coil. The four links affixed LG1, two positions in LG2, and the LG2/LG3 junction to a single α subunit residue, α K2119, indicating that much of the cloverleaf is near the α side of the coiled-coil base but does not bury position K2119.

No cross-links between the LG domains and the β and γ coiled-coil regions were observed, but a short carboxyl-terminal tail of the γ subunit downstream of the coiled coil was cross-linked to LG domains. Specifically, residue γ K1606, the second to last amino acid of the γ subunit, was linked to LG1 (α K2277) and LG2 (α K2467). K1606 is adjacent to a conserved glutamate (γ E1605) (Fig. 6), shown previously to be crucial for integrin binding (45). The cross-linking results support a model in which the γ chain tail is in the vicinity of the LG1/LG2 interface and may assist in forming the cloverleaf association, explaining why the crystal structure of LG1 through LG3, which lacked the coiled coil and γ chain tail, did not form the cloverleaf and why removal of γ E1605 undermined integrin binding (45). The LG docking models and observed interactions with residues near the coiled-coil terminus, while yielding only approximate orientations, nevertheless provide molecular insight into self-assembly of cell-binding regions of laminin.

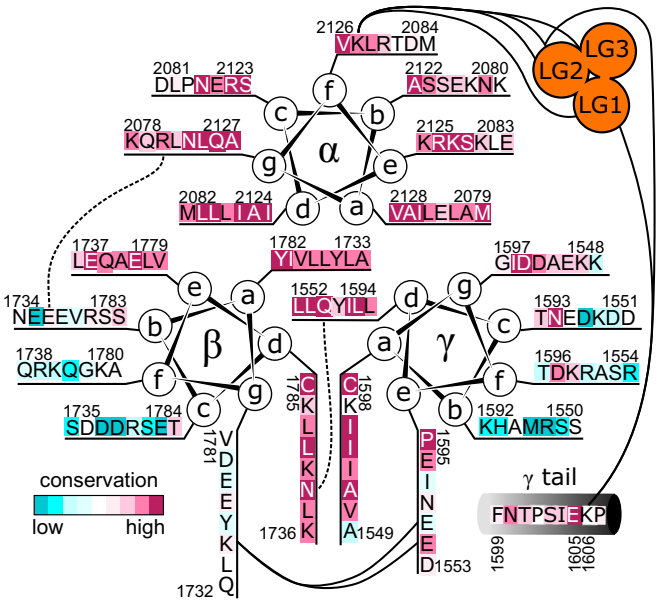

Fig. 6. Carboxyl terminus of the laminin coiled coil. Helical wheels with residues colored according to conservation (50). The γ subunit segment downstream of the coiled coil (γ tail) is also displayed. Solid curves indicate cross-links, and dashed curves indicate proposed interactions discussed in the text. Conservation scores for the entire laminin coiled coil are in Figs. S7–S9.

Discussion

To map the laminin quaternary structure, we sought to obtain intersubunit cross-links densely and extensively over the assembly. By use of three cross-linking chemistries, we obtained 69 cross-links between subunits in the coiled coil. It is likely that more cross-links formed but remained undetected by MS because of nonoptimal peptide properties, such as length or post-translational modification (Figs. S5 and S6). From the data acquired, certain key regions, such as the carboxyl terminus of the coiled coil, were directly highly constrained (Fig. 6 and Fig. S1). In contrast, other regions were somewhat underdetermined. Due to the BS3 and SDH linker lengths, each cross-link fixes the register within only about three heptads to either direction. Greater insight was obtained, however, by developing new tools to integrate information from multiple cross-links. Coarse-grained molecular dynamics simulations in the context of coiled-coil geometry and heptad prediction maximized the information extractable from the entire experimental dataset (Fig. 5). This approach yielded a chain register prediction to within two heptads over most of the coiled-coil length, which was sufficient to achieve insights into laminin assembly and will help guide future studies of laminin interactions with other proteins.

One of the central issues underlying laminin structure is the order of the three subunits in the coiled coil. In the laminin assembly mechanism, β and γ are proposed to form a preliminary heterodimer, onto which α docks to complete the trimer (46). Therefore, the subunit order is determined by which side of the β-γ interface the α subunit binds. Two major determinants of the preferred order are the geometric packing of residues at **a** and **d** positions and electrostatic interactions among other positions, primarily **e** and **g**. A previous attempt at assigning the chain order was based on electrostatics; in the absence of information on subunit register, the alignment was adjusted to optimize intersubunit ionic interactions (24). Our approach, which was independent of subunit register and relied on experimental data, led to the opposite conclusion regarding the subunit order: a counterclockwise arrangement of α, β, and γ when viewed from the carboxyl terminus (Fig. 3).

The chain order established herein supports the subunit arrangement accompanying a suggested mechanism for the multistep assembly of laminin trimers (27). However, the heptad position assignment in the suggested mechanism differs somewhat from our prediction (Fig. 6). In particular, the β subunit is rotated by one position and shifted by half a heptad. It is noteworthy that the tension between these two heptad and register assignments may reflect a key aspect of laminin structure. Whereas both models for the carboxyl terminus of the laminin coiled coil were based on an ideal, symmetric trimer (27) (Fig. 6), the laminin heterotrimer is most probably asymmetric, leading to deviations from the convention in which only **a** and **d** positions participate directly in coiled-coil core interactions.

Irregularities in hetero-oligomeric coiled coils may be the rule rather than the exception and may contribute both to function and to specificity of assembly. The blood clotting factor fibrinogen, which contains a coiled coil spanning about 160 Å, is currently the most extensive source of structural information on heterotrimeric coiled-coil assembly. X-ray crystal structures of fibrinogen reveal kinks, asymmetric superhelix crossing angles, and short, nonhelical segments looping out of the coiled coil (39, 40). Notably, glycines are accommodated with no disruption to coiled-coil helices, single prolines are accommodated with a minor kink, and two prolines separated by six intervening residues are observed to locally break the helix. Laminin may accommodate such sequence features in a similar manner. The laminin γ subunit contains a moderately conserved proline pair separated by four to seven amino acids, whereas β contains a highly conserved proline pair separated by two intervening amino acids. Although paired proline residues are indeed likely to cause local disruptions in the helix, fragmentation in laminin coiled-coil potential predictions (21) may not always indicate actual breaks in the helical assembly. Fibrinogen demonstrates how local aberrations may produce kinks or bends without undermining the coiled-coil framework.

The analyses presented in this study were based on a threefold symmetric, ideal coiled coil as a starting model. Notably, the two competing chain arrangements for α, β, and γ could be distinguished robustly using the cross-linking data interpreted on the backdrop of the ideal trimer (Fig. 3). For more subtle insights into heptad position assignments and register determination of specific coiled-coil regions, conflict between the cross-linking data and the ideal model can be exploited. For example, we found two neighboring zero-length cross-links between β and γ that were inconsistent with a continuous heptad repeat between them. These cross-links were between β subunit **g**-position residues E1725 and K1746 and γ residues K1544 and E1560, assigned by MARCOIL as **c** and **e** positions, respectively. According to standard coiled-coil geometry, **g** positions can form direct links to **e** or possibly **b** positions, but not **c** positions. Thus, a conflict between cross-linkability and ideal coiled-coil geometry arises. We interpret the cross-linking results to indicate deviations from ideal geometry and heptad continuity in this region.

In addition to the cross-links introduced into laminin in this study, a natural cross-link clamps the coiled-coil base: a disulfide bond links the β and γ subunits near their carboxyl termini (46). A disulfide similarly bridges two subunits at the fibrinogen coiled coil (39, 40). With the caveat that the laminin disulfide may lie outside the region that is formally a coiled coil, it should constrain the β/γ subunit register. Indeed, the introduction of cysteine residues into coiled coils has been used as an experimental strategy to determine coiled-coil register (47). In the fibrinogen structure, the bonded cysteines are at **d** and **a** positions. The corresponding laminin cysteines were previously proposed to be at **g** and **a** positions in β and γ (27). If the laminin coiled coil includes the disulfide, our cross-linking data suggest that the cysteines would be at **d** and **a** positions in β and γ, respectively, comparable to the fibrinogen positioning.

We present here a definitive experimental determination of the subunit order and a prediction of the subunit register for the laminin coiled coil. In addition, we obtained insights into the location of the Lβ knob with respect to the other coiled-coil subunits and into the association of LG domains with the carboxyl terminus of the coiled coil, a requirement for integrin binding (45). The functional importance of the laminin protein family in interaction and signaling between cells and the ECM warrants continued efforts to explore the structure and dynamics of this remarkable macromolecule. The data and analyses presented herein will facilitate future high-resolution structural studies of additional laminin segments. The methods described in this work extend the application and impact of cross-linking and mass spectrometry to proteins with repetitive structures that can be parameterized, including many proteins in the cell microenvironment. These proteins have been the focus of numerous molecular and cell biology studies, but they continue to be recalcitrant to high-resolution structure determination in their full-length, native assemblies.

Materials and Methods

Laminin-111 was purchased from Gibco and cross-linkers from Creative Molecules. Cross-linking reactions, MS data acquisition, MS and amino acid sequence analyses, and the design and execution of cross-link–constrained simulations are described in *SI Materials and Methods*. MS data have been deposited in the ProteomeXchange Consortium via the PRIDE (48) partner repository with the dataset identifier PXD004898.

ACKNOWLEDGMENTS. We thank E. Levy for critical reading of the manuscript and helpful suggestions. D. Merhav and D. Elinger prepared samples for MS. H. Greenblatt and K. Levy group members provided infrastructure for simulations. This work was supported by a grant from the Israel Science Foundation, the European Research Council under the European Union's Seventh Framework Programme, Grant 310649, and the Israeli Center of Research Excellence (I-CORE) in Structural Cell Biology.

1. Miner JH (2008) Laminins and their roles in mammals. *Microsc Res Tech* 71(5):349–356.
2. Hohenester E, Yurchenco PD (2013) Laminins in basement membrane assembly. *Cell Adhes Migr* 7(1):56–63.
3. Hynes RO (2012) The evolution of metazoan extracellular matrix. *J Cell Biol* 196(6):671–679.
4. Edwards MM, Lefebvre O (2013) Laminins and retinal vascular development. *Cell Adhes Migr* 7(1):82–89.
5. Laperle A, et al. (2015) α-5 laminin synthesized by human pluripotent stem cells promotes self-renewal. *Stem Cell Rep* 5(2):195–206.
6. Pradhan S, Farach-Carson MC (2010) Mining the extracellular matrix for tissue engineering applications. *Regen Med* 5(6):961–970.
7. Patarroyo M, Tryggvason K, Virtanen I (2002) Laminin isoforms in tumor invasion, angiogenesis and metastasis. *Semin Cancer Biol* 12(3):197–207.
8. Candiello J, Cole GJ, Halfter W (2010) Age-dependent changes in the structure, composition and biophysical properties of a human basement membrane. *Matrix Biol* 29(5):402–410.
9. Engel J, et al. (1981) Shapes, domain organizations and flexibility of laminin and fibronectin, two multifunctional proteins of the extracellular matrix. *J Mol Biol* 150(1): 97–120.
10. Aumailley M, et al. (2005) A simplified laminin nomenclature. *Matrix Biol* 24(5):326–332.
11. Kammerer RA, et al. (1999) Interaction of agrin with laminin requires a coiled-coil conformation of the agrin-binding site within the laminin γ1 chain. *EMBO J* 18(23): 6762–6770.
12. Colognato-Pyke H, et al. (1995) Mapping of network-forming, heparin-binding, and α 1 β 1 integrin-recognition sites within the α-chain short arm of laminin-1. *J Biol Chem* 270(16):9398–9406.
13. Tisi D, Talts JF, Timpl R, Hohenester E (2000) Structure of the C-terminal laminin G-like domain pair of the laminin α2 chain harbouring binding sites for α-dystroglycan and heparin. *EMBO J* 19(7):1432–1440.
14. Harrison D, et al. (2007) Crystal structure and cell surface anchorage sites of laminin α1LG4-5. *J Biol Chem* 282(15):11573–11581.
15. Carafoli F, Clout NJ, Hohenester E (2009) Crystal structure of the LG1-3 region of the laminin α2 chain. *J Biol Chem* 284(34):22786–22792.
16. Hussain SA, Carafoli F, Hohenester E (2011) Determinants of laminin polymerization revealed by the structure of the α5 chain amino-terminal region. *EMBO Rep* 12(3):276–282.
17. Carafoli F, Hussain SA, Hohenester E (2012) Crystal structures of the network-forming short-arm tips of the laminin β1 and γ1 chains. *PLoS One* 7(7):e42473.
18. Moran T, Gat Y, Fass D (2015) Laminin L4 domain structure resembles adhesion modules in ephrin receptor and other transmembrane glycoproteins. *FEBS J* 282(14):2746–2757.
19. Stetefeld J, Mayer U, Timpl R, Huber R (1996) Crystal structure of three consecutive laminin-type epidermal growth factor-like (LE) modules of laminin γ1 chain harboring the nidogen binding site. *J Mol Biol* 257(3):644–657.
20. Takagi J, Yang Y, Liu JH, Wang JH, Springer TA (2003) Complex between nidogen and laminin fragments reveals a paradigmatic β-propeller interface. *Nature* 424(6951):969–974.
21. Zimmerman T, Blanco FJ (2007) The coiled-coil structure potential of the laminin LCC domain is very fragmented and does not differentiate between natural and non-detected isoforms. *J Biomol Struct Dyn* 24(4):413–420.
22. Barlow DP, Green NM, Kurkinen M, Hogan BL (1984) Sequencing of laminin B chain cDNAs reveals C-terminal regions of coiled-coil α-helix. *EMBO J* 3(10):2355–2362.
23. Paulsson M, et al. (1985) Evidence for coiled-coil α-helical regions in the long arm of laminin. *EMBO J* 4(2):309–316.
24. Beck K, Dixon TW, Engel J, Parry DAD (1993) Ionic interactions in the coiled-coil domain of laminin determine the specificity of chain assembly. *J Mol Biol* 231(2):311–323.
25. Yurchenco PD (2011) Basement membranes: Cell scaffoldings and signaling platforms. *Cold Spring Harb Perspect Biol* 3(2):a004911.
26. Domogatskaya A, Rodin S, Tryggvason K (2012) Functional diversity of laminins. *Annu Rev Cell Dev Biol* 28:523–553.
27. Nomizu M, et al. (1996) Mechanism of laminin chain assembly into a triple-stranded coiled-coil structure. *Biochemistry* 35(9):2885–2893.
28. Walzthoeni T, Leitner A, Stengel F, Aebersold R (2013) Mass spectrometry supported determination of protein complex structure. *Curr Opin Struct Biol* 23(2):252–260.
29. Merkley ED, Cort JR, Adkins JN (2013) Cross-linking and mass spectrometry methodologies to facilitate structural biology: Finding a path through the maze. *J Struct Funct Genomics* 14(3):77–90.
30. Barysz H, et al. (2015) Three-dimensional topology of the SMC2/SMC4 subcomplex from chicken condensin I revealed by cross-linking and molecular modelling. *Open Biol* 5(2):150005.
31. Aumailley M (2013) The laminin family. *Cell Adhes Migr* 7(1):48–55.
32. Rinner O, et al. (2008) Identification of cross-linked peptides from large sequence databases. *Nat Methods* 5(4):315–318.
33. Leitner A, et al. (2014) Chemical cross-linking/mass spectrometry targeting acidic residues in proteins and protein complexes. *Proc Natl Acad Sci USA* 111(26):9455–9460.
34. Kahraman A, Malmström L, Aebersold R (2011) Xwalk: Computing and visualizing distances in cross-linking experiments. *Bioinformatics* 27(15):2163–2164.
35. Macdonald PR, Lustig A, Steinmetz MO, Kammerer RA (2010) Laminin chain assembly is regulated by specific coiled-coil interactions. *J Struct Biol* 170(2):398–405.
36. Grigoryan G, Degrado WF (2011) Probing designability via a generalized model of helical bundle geometry. *J Mol Biol* 405(4):1079–1100.
37. Delorenzi M, Speed T (2002) An HMM model for coiled-coil domains and a comparison with PSSM-based predictions. *Bioinformatics* 18(4):617–625.
38. Lupas AN, Gruber M (2005) The structure of α-helical coiled coils. *Adv Protein Chem* 70:37–78.
39. Yang Z, Kollman JM, Pandi L, Doolittle RF (2001) Crystal structure of native chicken fibrinogen at 2.7 A resolution. *Biochemistry* 40(42):12515–12523.
40. Kollman JM, Pandi L, Sawaya MR, Riley M, Doolittle RF (2009) Crystal structure of human fibrinogen. *Biochemistry* 48(18):3877–3886.
41. Mascarenhas JB, et al. (2003) Mapping of the laminin-binding site of the N-terminal agrin domain (NtA). *EMBO J* 22(3):529–536.
42. Utani A, Nomizu M, Timpl R, Roller PP, Yamada Y (1994) Laminin chain assembly. Specific sequences at the C terminus of the long arm are required for the formation of specific double- and triple-stranded coiled-coil structures. *J Biol Chem* 269(29):19167–19175.
43. Bruch M, Landwehr R, Engel J (1989) Dissection of laminin by cathepsin G into its long-arm and short-arm structures and localization of regions involved in calcium dependent stabilization and self-association. *Eur J Biochem* 185(2):271–279.
44. de Vries SJ, van Dijk M, Bonvin AM (2010) The HADDOCK web server for data-driven biomolecular docking. *Nat Protoc* 5(5):883–897.
45. Ido H, et al. (2007) The requirement of the glutamic acid residue at the third position from the carboxyl termini of the laminin γ chains in integrin binding by laminins. *J Biol Chem* 282(15):11144–11154.
46. Hunter I, Schulthess T, Engel J (1992) Laminin chain assembly by triple and double stranded coiled-coil structures. *J Biol Chem* 267(9):6006–6011.
47. Weitzel CS, Waldman VM, Graham TA, Oakley MG (2011) A repeated coiled-coil interruption in the *Escherichia coli* condensin MukB. *J Mol Biol* 414(4):578–595.
48. Vizcaíno JA, et al. (2016) 2016 update of the PRIDE database and its related tools. *Nucleic Acids Res* 44(D1):D447–D456.
49. Combe CW, Fischer L, Rappsilber J (2015) xiNET: Cross-link network maps with residue resolution. *Mol Cell Proteomics* 14(4):1137–1147.
50. Glaser F, et al. (2003) ConSurf: Identification of functional regions in proteins by surface-mapping of phylogenetic information. *Bioinformatics* 19(1):163–164.
51. Leitner A, Walzthoeni T, Aebersold R (2014) Lysine-specific chemical cross-linking of protein complexes and identification of cross-linking sites using LC-MS/MS and the xQuest/xProphet software pipeline. *Nat Protoc* 9(1):120–137.
52. Altschul SF, et al. (1997) Gapped BLAST and PSI-BLAST: A new generation of protein database search programs. *Nucleic Acids Res* 25(17):3389–3402.
53. Edgar RC (2004) MUSCLE: Multiple sequence alignment with high accuracy and high throughput. *Nucleic Acids Res* 32(5):1792–1797.
54. Azia A, Levy Y (2009) Nonnative electrostatic interactions can modulate protein folding: Molecular dynamics with a grain of salt. *J Mol Biol* 393(2):527–542.